Nanoscale

Dynamic Article Links ▶

ARTICLE TYPE

Mesoporous Titania Based Yolk-Shell Nanoparticles as Multifunctional Theranostic Platforms for SERS Imaging and Chemo-Photothermal Treatment

Weiwei Zhang,[†§] **Yunqing Wang,**[§]* **Xiuyan Sun,**[†] **Wenhai Wang,**[§] **and Lingxin Chen**[§]*

Recently surface-enhanced Raman scattering (SERS) imaging guided theranostic nanoplatforms have attracted considerable attention. Herein, we developed novel yolk-shell gold nanorod@void@mesoporous titania nanoparticles (AuNR@void@mTiO$_2$ NPs) for simultaneous SERS imaging and chemo-
10 photothermal therapy. Our work showed three highlighted features: First, we proposed a facile and versatile "up to down" SERS labeling strategy for drug delivery system, in which "empty carriers" were pre-synthesized, followed by co-loading of Raman reporters on AuNR and anti-cancer drugs doxorubicin (DOX) in mTiO$_2$ in sequence. The acquired SERS signal was strong enough for NPs tracking at both living cells and mice levels. Second, we selected mTiO$_2$ as novel drug loading material instead of the
15 widely used mesoporous silica (mSiO$_2$). The mTiO$_2$ shared satisfactory drug loading and release behavior as mSiO$_2$ but it was much chemical inert. This property not only provided a facial way to form yolk-shell structure but also rendered it superior structural stability in biological system. Third, the near infrared (NIR) light absorbing property of AuNR SERS substrate was also explored for drug release regulation and photothermal treatment. Significantly greater MCF-7 cell killing was observed when treated together
20 with DOX-loaded NPs and NIR laser irradiation, attributable to the synergistic chemo-thermal therapeutic effect. Our results indicated established SERS labeled yolk-shell NP as a promising theranostic platform and suggested its potential *in vivo* applications.

1. Introduction

25 The development of various kinds of nanomaterials with unique physico-chemical properties has offered an opportunity to devise multifunctional nanoplatforms that integrate different theranostic modalities for simultaneous disease treatment and real-time diagnosis.[1, 2] Chemo-photothermal therapeutic systems based on
30 some remote-activated, near infrared (NIR) light absorbing photothermal nanoparticles (NPs) draw much attention in recent years.[3, 4] Upon NIR light irradiation, the heat generated from these materials can not only kill cancer cells but also modulate drug release for chemotherapeutics. Therefore, an enhanced
35 treating efficacy is achieved by the synergistic effects of heat and drug target-released at the tumor sites.[5]

Apart from curing disease, the function of diagnosis is another major concern in the development of theranostic nanoplatforms. As a newly arising optical detection technique,
40 surface-enhanced Raman scattering (SERS) imaging is considered an ideal diagnostic mode utilized for the construction of theranostic systems.[6-10] On one hand, SERS imaging possesses many advantages over traditional NIR fluorescence and magnetic resonance imaging for the high sensitivity, tremendous
45 multiplexing capacity, quantification capability, and high

photostability,[11, 12] which have been successfully applied for biological imaging analysis at the level of live-cell, tissues and living small animals.[11, 13, 14] On the other hand, many noble metal NP based SERS nanosubstrates such as gold nanorod (AuNR),[15,
50 16] gold nanocage[17] and gold nano-popcorn,[18] are also satisfactory photothermal agents. The bi-function makes it possible to combine SERS image-guided diagnosis, hyperthermia and chemotherapeutics within a relative simple nanoplatform of few compositions.

55 Despite noble metal NPs owned the above mentioned bi-functions, they still suffer from two drawback as drug delivery systems. The first is their relatively low specific surface area limits the loading amount of drugs. The second is that they trend to aggregate after loading drug or entering cells, which induces
60 maximum spectral absorption shifting and the decrease of photothermal efficacy.[19] To overcome these problems, additional coating was usually applied to increase the colloidal stability and drug molecule storage capacity. For instance, mesoporous silica coated gold nanorod (AuNR@mSiO$_2$) was synthesized for anti-
65 cancer drug doxorubicin (DOX) loading and chemo-photothermal treatment for tumor.[3, 19, 20] However, many coating conditions, such as the application of organic solvents, high concentration of

CTAB or extreme pH adjustment usually cause Raman reporter detaching from noble metal NP, resulting in the pre-generated SERS signal disappeared. Therefore, a more versatile nanostructure and a robust SERS signal generation strategy should be explored.

Yolk-shell NPs are a special class of core-shell nanostructures with unique properties of movable cores, interstitial hollow spaces between the movable core and shell sections, which were considered as interesting candidates for developing drug delivery system.[21] We speculated yolk-shell NPs held great potential for the construction of SERS-based theranostic systems owing to the structural characteristics, in which noble metal NPs and mesoporous shells could be separated by interior hollow, thus SERS generation and drug loading could be realized without interference. With this idea in mind, we devised novel multifunctional $AuNR@void@mTiO_2$ yolk-shell NPs, in which NIR light absorbing AuNR inner core serving as bi-functions of SERS substrate and photothermal agent, and mesoporous titania ($mTiO_2$) outer shell being for drug loading.[22] The synthetic procedure was represented in **Scheme 1**. In brief, the whole process involved: 1) the synthesis of $AuNR@mSiO_2$ NPs; 2) a further coating of $mTiO_2$ on multiple $AuNR@mSiO_2$ NPs to form a $AuNR@mSiO_2@mTiO_2$ nanostructure; 3) the controllable etching of the interior $mSiO_2$ layer with NaOH to produce $AuNR@void@mTiO_2$ yolk-shell NPs; 4) Raman reporter molecules penetrating through $mTiO_2$ shell, attaching on AuNR via diffusion process in acidic condition for SERS signal generation; 5) the loading of DOX in $mTiO_2$ at neutral pH environment, endowing NPs with chemotherapeutic functions. Finally, to demonstrate the multifunction, the SERS imaging and chemo-photothermal therapeutic effects were tested upon irradiation of NIR laser.
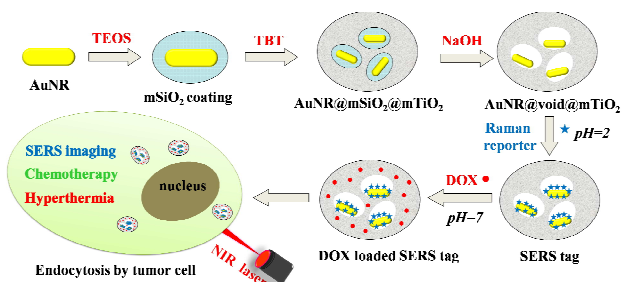
Scheme 1. Synthesis of $AuNR@void@mTiO_2$ yolk-shell NPs as multifunctional theranostic platforms for cancer treatment.

2. Experimental

2.1. Materials

Chloroauric acid ($HAuCl_4 \cdot 3H_2O$), silver nitrate ($AgNO_3$), sodium borohydride ($NaBH_4$), sodium hydroxide (NaOH) L-ascorbic acid (AA), crystal violet, tetraethoxyorthosilicate (TEOS) and tetrabutyl titanate (TBT) were purchased from Sinopharm Chemical Reagent Co., Ltd. Nonionic surfactant Lutensol ON50 was obtained from BASF. Cetyltrimethyl ammonium bromide (CTAB), doxorubicin hydrochloride (DOX), 3,3'-diethylthiadicarbocyanine iodine (DTDC) and 3,3'-diethylthiatricarbocyanine iodide (DTTC) were obtained from

Sigma–Aldrich. 5-carboxyfluorescein diacetate (CFDA) and propidium iodide (PI) were obtained from Aladdin Industrial Co., Ltd. MTT (3-(4,5-dimethylthiazol-2-yl)-2,5-diphenyltetrazolium bromide) was purchased from Invitrogen. RPMI-1640 medium, fetal bovine serum, penicillin-streptomycin solution and trypsin-EDTA solution were purchased from Thermo Scientific. Deionized water was used in all of the experiments.

2.2. Characterization

The TEM images were acquired on a JEM-1400 transmission electron microscope (JEOL, Japan). The SEM images were obtained on an S-4800 field emission scanning electron microscope (Hitachi, Japan). UV/Vis/NIR absorption spectra were recorded on a Thermo Scientific NanoDrop 2000/2000C spectrophotometer. SERS spectra were recorded by using a DXR Raman Microscope (Thermal Fisher, USA). A 632.8 nm He:Ne laser was focused by a ×10 and ×50 microscope objective for sample solution and cell measurement, respectively, with a power of 2 mW. Confocal laser scanning microscopy (CLSM) was operated on an Olympus Fluoview FV1000 (Japan). The hydrodynamic diameters and zeta potentials of the NPs were measured on a Zetasizer Nano ZS90 (Malvern, U.K.) in water medium.

2.3. Preparation of AuNRs

AuNRs were synthesized by using the seed-mediated growth method.[23] Briefly, the seed solution was prepared by reducing $HAuCl_4$ (0.5 mM, 2 mL) in CTAB (0.2 M, 2 mL) with freshly prepared ice-cold $NaBH_4$ (10 mM, 0.24 mL). After 2 h, 3.6 mL of resultant seed solution was added into a growth solution of $HAuCl_4$ (23 mM, 13 mL), CTAB (0.2 M, 200 mL), $AgNO_3$ (4 mM, 11.2 mL), and AA (0.08 M, 5 mL). The mixture was left overnight at 27-30 ℃.

2.4. Preparation of AuNR@mSiO₂ NPs

$AuNR@mSiO_2$ NPs were synthesized according to a published procedure with some minor modifications.[24] The as-prepared AuNRs (40 mL) were centrifuged (9500 r, 25 min) and dispersed in water (20 mL), followed by addition of NaOH (0.1 M, 200 µL) under stirring. Then, 20% TEOS in ethanol (180 µL) was added for three times at intervals of 30 min under mixing. The resulting solution was further allowed to react for 48 h at 26-28 ℃. The obtained $AuNR@mSiO_2$ core-shell NPs were then collected and washed twice with water (9000 r, 15 min), once with ethanol (8500 r, 15 min), and then dispersed in 20 mL ethanol.

2.5. Preparation of AuNR@mSiO₂@mTiO₂ NPs

A typical procedure for coating $AuNR@mSiO_2$ particles with $mTiO_2$ is as follows.[25, 26] Firstly, a 0.1 M aqueous solution of Lutensol ON50 (4 µL) was dissolved in a pre-mixed dispersion of $AuNR@mSiO_2$ core particles (200 µL) in ethanol (300 µL). Then, a further 500 µL of ethanol was mixed with TBT (10 µL). This diluted titania precursor solution was then added to the dispersion of core particles, followed by vigorous shaking. The mixture was sonicated for at least 20 min in an ultrasound bath before being left overnight to allow the reaction to go to completion. The $AuNR@mSiO_2@mTiO_2$ NPs were washed twice (5000 r, 5 min) with ethanol and water and then dispersed in 250 µL water.

2.6. Preparation of AuNR@void@mTiO$_2$ NPs

A NaOH solution (0.5 M, 250 μL) was added to the AuNR@mSiO$_2$@mTiO$_2$ NP solution, and the mixture was kept for 2 h to selectively remove the mSiO$_2$. The resulting AuNR@void@mTiO$_2$ yolk-shell particles were isolated by centrifugation and washed three times with water (4000 r, 5 min), and finally dispersed in 500 μL water.

2.7. SERS signal generation

The pH of AuNR@void@mTiO$_2$ NP solution (500 μL) was adjusted to about 2 with concentrated hydrochloric acid before the addition of Raman reporter molecule DTDC (10^{-4} M, 50 μL). The mixture was kept for 30 min and then centrifuged (4000 r, 5 min) and washed twice with water and then dispersed in 500 μL water for SERS signal measurement.

2.8. Anti-cancer drug (DOX) loading

DTDC labeled NPs (500 μL) was centrifuged and redispersed into a solution of DOX in water (2×10^{-4} M, 500 μL). After different incubation times (5, 10, 20, 30, 40, 60 and 90 min), the NPs were centrifuged and the supernatant was subjected to UV/Vis analysis to determine the amount of loaded DOX. A stock solution of DOX (10^{-4} M) was used as a standard and was serially diluted to concentrations of 5.0-100×10^{-6} M in water. DOX solutions of different concentration were measured at 480 nm and a linear fit of the data was created and used as standard curve for the absorption against DOX concentration.

2.9. Photothermal property

1 mL of the AuNR@void@mTiO$_2$ NP solution (0.2 mg mL^{-1}) filled in a 1.5 mL Eppendorf tube was irradiated for 10 min by a NIR laser (785 nm, 400 mW) at a distance of 1 cm from the side of the solution. A thermoindicator was used to monitor the temperature change. Water was utilized as a negative control and AuNR with the same concentration was utilized as a positive control.

2.10. *In vitro* drug release

1.0 mL of DOX-loaded NP solution in PBS buffers with different pH (5.0, 7.4) was agitated at room temperature. The mixture was centrifuged at different time intervals. The supernatant was collected and the same volume of fresh buffers was added back to the residual. The amount of released drug in the supernatant was measured by a UV-Vis spectrometer at 480 nm. A similar procedure was applied in the NIR laser controlled drug release study. The NP buffer solution (pH 5.0) was irradiated with a NIR laser (785 nm, 400 mW) for 6 min. The supernatant was collected for UV-Vis measurement to study the DOX release behavior.

2.11. Mesoporous shell stability

AuNR@mSiO$_2$ and AuNR@void@mTiO$_2$ solution sample (1 mL for each) with the same AuNR concentration was centrifuged and further dispersed into pH 7.4 PBS buffer (0.01 M, 1 mL). The mixtures were gently stirred at a constant temperature of 37 °C. The NPs were centrifuged and collected at different intervals for morphology observation via SEM.

2.12. Cell culture

A breast-cancer-cell line (MCF-7) was grown as a monolayer in a humidified incubator at 37 °C in air/CO$_2$ (95:5) in an RPMI-1640 medium that was supplemented with 10% fetal bovine serum. For all experiments, the cells were harvested by using trypsin and were resuspended in fresh medium before plating.

2.13. Cell imaging

MCF-7 cells (2.0×10^4) were seeded onto glass cover-slips in a 24-well plate with 540 μL culture medium to allow the cells to attach. Then a 60 μL of DOX-loaded yolk-shell NP solution (20 μg mL^{-1}, with 1 μM DOX) was added into the cells. After incubation for different times, the cell monolayer on the cover-slip was repeatedly washed with PBS to remove the remaining particles and dead cells and then sealed with a glass microscope slide. Observations were performed by confocal laser scanning microscopy and Raman microscopy.

2.14. *In vivo* SERS detection

100 μL of the DOX-loaded NP solution was injected subcutaneously at the abdomen of an anaesthetized Kunming mouse. The subcutaneous SERS spectrum was detected using an Agility Raman spectrometer (BaySpec, USA). The laser power was 200 mW and the integration time was 1 s. The control spectrum was taken in an area away from the injected site.

2.15. Therapeutic effect assessment

8×10^3 MCF-7 cells were plated in 96-well plates and incubated for 24 h to allow the cells to attach. AuNR@void@mTiO$_2$ yolk-shell NPs were added into the cells to form NP suspensions in culture media with different concentrations (0, 1, 5, 10, 20, 40, 60, 80 and 120 μg mL^{-1}). Then, the cells were incubated at 37 °C for another 24 h. Cell viability of the blank nanocarriers (before loading drugs) was evaluated by using an MTT assay. Thereafter, in a separate experiment, the cells were exposed to free DOX and DOX-loaded NPs with NP concentration of 10 μg mL^{-1} and DOX concentration of 1 μM. The cells were or were not irradiated by NIR laser (6.25 W cm^{-2}) with illumination for 5 min after 6 h' drug incubation. Then the cells were incubated at 37 °C for another 24 h. The cells were washed with PBS buffer, submerged in 500 μL PBS, examined under a fluorescence microscope using a live-cell staining procedure consisting 5-carboxyfluorescein diacetate (CFDA, 100 μg mL^{-1} in PBS, 10 μL) and propidium iodide (PI, 30 μg mL^{-1} in PBS, 7.5 μL). Non-fluorescent CFDA can be converted to green fluorescent 5-carboxyfluorescein (with 495 nm laser irradiation) by esterases in living cells. Membrane impermeant PI enters dead cells and displayed enhanced red fluorescence when binds to DNA/RNA. Then, the effects of exposure to laser, DOX and the multifunctional NPs were quantitatively evaluated by using MTT assays.

3. Results and discussion

3.1. Synthesis of AuNR@void@mTiO$_2$ Yolk-shell NPs

The TEM image of AuNR (**Fig.1a**) showed that the average length and width were around 43 nm and 12 nm, respectively (about 3.6:1 aspect ratio). The TEM images of AuNR@mSiO$_2$ NPs (**Fig. 1b**) indicated that each AuNR was coated with a uniform mSiO$_2$ shell of 15 nm thickness and these core-shell NPs were uniform and well-dispersed. During mTiO$_2$ coating process,

it was found that the concentration of AuNR@mSiO$_2$ core NPs affected the shape of the products. When the amount of core NPs was 200 μL in a 1.0 mL reaction mixture, the resultant mTiO$_2$ coated NPs were sphere like with the particle size around 250 nm (**Fig. 1c,d**). Dynamic light scattering measurement revealed a reasonable, a little larger hydrodynamic diameter in the range of 250 nm to 450 nm (**Fig. S1**). When the volume of core NPs was increased to 500 μL, a nonuniform "worm-shaped" structure was obtained (**Fig. S2a,b**). It had been reported that mTiO$_2$ structure synthesized with Lutensol ON50 had a Barret-Joyner-Halenda adsorption average pore diameter of 1.68 nm,[27] which provided a precondition for the subsequent NaOH penetration and resultant mSiO$_2$ etching process. Under basic condition, mSiO$_2$ in the middle layer was dissolved by weakening the siloxane bonds and coordinating OH$^-$ ions to Si atoms, while outer mTiO$_2$ shell was kept compact due to its chemical inertness,[28, 29] thus a yolk-shell NP structure could be formed. High-magnification TEM image of nanosphere NP in **Fig. 1d** showed the pale rings around multiple AuNRs, indicating gaps between AuNR and mTiO$_2$. For nanoworm NPs the yolk-shell structure was much easier to be observed due to relative thin mTiO$_2$ shell (**Fig. S2c**). This yolk-shell NP structure simply achieved by tactfully taking advantage of the stability difference of mSiO$_2$ and mTiO$_2$, avoiding multi-steps or the application of high temperature and non-green etching agents.[30] Considering the demand of uniformity and drug loading capacity of nanomedicine, sphere like yolk-shell structures with thicker mTiO$_2$ shell was used in the following study.
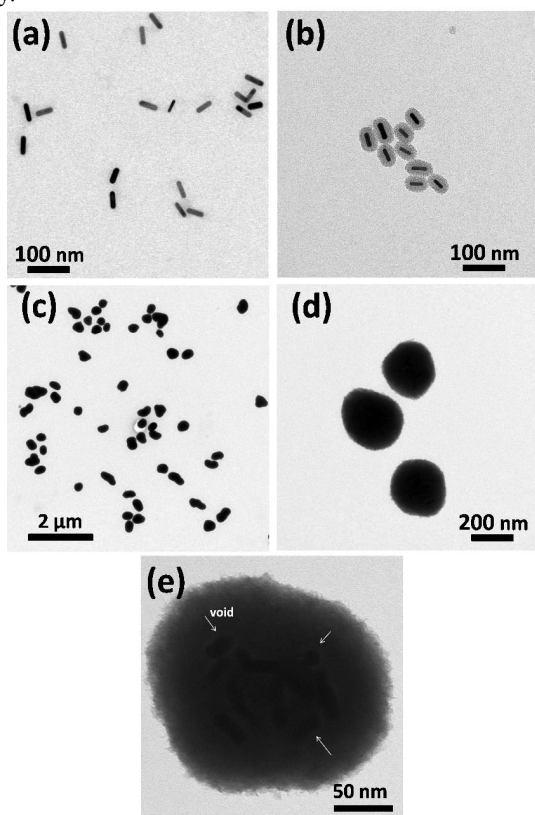

Fig. 1. TEM images of AuNR (a), AuNR@mSiO$_2$ (b) and sphere like AuNR@mSiO$_2$@mTiO$_2$ NPs (c, d). (e) showed a high resolution TEM image of a AuNR@void@mTiO$_2$ yolk-shell nanosphere. The white arrows indicated the gaps between AuNRs and mTiO$_2$.

3.2. Optical Characterization of AuNR@void@mTiO$_2$ NPs

As shown in **Fig. 2a**, the longitudinal localized surface plasmon resonance (SPR) band of AuNR@mSiO$_2$ red shifted about 20 nm (from 764 nm to 784 nm) comparing with the absorption spectrum of bare AuNR. This could be explained by the fact that the local refractive index of the silica shell (1.45) was larger than water (1.33).[31] Interestingly, after dissolving mSiO$_2$, the "spaced" mTiO$_2$ shell had similar red-shift effect as the adhered mSiO$_2$ to AuNR and yolk-shell NPs still showed a longitudinal SPR absorption at 784 nm. Meanwhile, a strong end-absorption at 272 nm appeared, which was attributed to UV light absorption of mTiO$_2$ coating.

To render the NP SERS signals, we further investigated the Raman reporter labeling strategy. In general, the signal of SERS tags was usually produced following the sequence of noble metal NP preparation, Raman reporter attachment, and surface protection, which was regarded as a "bottom-up" way. However, for the production of SERS labeled multifunctional nanomedicine, this sequence would induce problems because the pre-generated SERS disappeared because several severe synthesis conditions (high concentration of CTAB at mSiO$_2$ coating process and NaOH etching stage) could detach Raman reporters from metal substrates. Herein, we proposed a versatile "up-down" strategy, in which SERS nanosubstrate were pre-stabilized by polymers[32] or mesoporous materials,[33, 34] followed by Raman reporters' subsequent mixing and infiltration step. In our cast, it was crucial to load Raman reporter DTDC and therapeutic drug DOX at proper positions of the nanoplatform (on AuNR and in mTiO$_2$, respectively), which determined the optical and therapeutic properties. To achieve this goal, we firstly tried a simple signal generation condition to mix the yolk-shell NPs and the DTDC solution in neutral pH. As shown in **Fig. S3a**, the apparent color change from brown to purple of NP solution indicated that a large amount of DTDC was adsorbed in mTiO$_2$ via strong electrostatic interaction. The strong fluorescence background from DTDC overwhelmed the SERS signals (**Fig. S3b**). In order to decrease this unwanted electrostatic interaction, we tested another way to adjust the pH of NP solution to about 2 before incubation with DTDC. As shown in **Fig. 2b**, after washing and dispersing NPs in water, characteristic and "clean" DTDC SERS signal was obtained from NP solution without fluorescence background under irradiation of 632.8 nm laser.[35] Two reasons contributed to this fortunate result: 1) In this acidic condition, most Ti-OH groups would be protonated, which could prevent the adsorption and facilitate positive charged DTDC to penetrate through the mTiO$_2$ shell to access AuNR surface. This fluorescence quenched state suggested the loaded DTDC was mostly on the surface of AuNR but not in mTiO$_2$.[7] 2) AuNR still maintained strong affinity to the Raman reporter via stable Au-N and Au-S bonds in such acidic medium. Therefore, after DTDC attachment, the SERS labeled yolk-shell NPs could still preserve the unoccupied mTiO$_2$ shells for further drug molecule loading. We also tested another two commonly used Raman reporters, i.e., crystal violet and DTTC, for SERS signal generation of our yolk-shell NPs. As shown in **Fig. S4**, the final products exhibited characteristic Raman signature of the corresponding Raman reporter, indicating that the method was versatile provided the chemical structure of Raman reporter was stable in acidic condition. To test whether

the drug loading affect the SERS signal, we loaded DOX in mTiO$_2$ shell at neutral pH, and it did not cause apparent variation of the SERS profile (**Fig. 2b**, the red line).
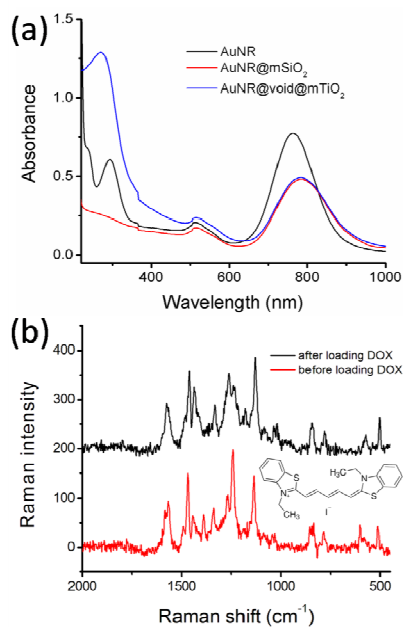

Fig. 2. (a) UV/Vis/NIR absorption spectra of AuNR, AuNR@mSiO$_2$ and AuNR@void@mTiO$_2$ NPs in water. (b) SERS spectra of DTDC labeled AuNR@void@mTiO$_2$ before and after loading DOX. The inset shows the
10 molecular structure of Raman reporter DTDC.

3.3. Photothermal Property of NPs

The AuNR@void@mTiO$_2$ NPs exhibited a high NIR absorption
15 from 700 to 900 nm, making it a potential photothermal treatment agent. As shown in **Fig. 3a**, under irradiation of a 785 nm NIR laser at a power 400 mW for 10 min, pure AuNR showed the best heat converting efficiency, with the temperature increased from 25 °C to 55 °C. Our AuNR@void@mTiO$_2$ NP solution also
20 showed dramatic temperature change from 25 °C to 51 °C. AuNR@void@mTiO$_2$ NP showed a little weaker efficacy than AuNR, which was because mTiO$_2$ shell around the AuNR affected light absorption and local heat diffusion in solution to some extent. As a negative control, the temperature of water was
25 stable at 25 °C. After 10 min treatment, the absorption spectrum of the samples was unchanged, indicating the AuNR cores was stable and not melt under this laser irradiation condition.

3.4. Drug Loading and Release Behaviors

Recently, mTiO$_2$ NPs had been found to be promising vehicles
30 for intracellular drug delivery,[22, 26, 36] and we further investigated the drug loading and release behaviors of the mTiO$_2$ shell in the yolk-shell NPs. **Fig. 3b** showed the UV/Vis absorption spectra of an aqueous solution of DOX before and after the interaction with SERS labeled NPs. The absorption intensity of DOX decreased
35 significantly, indicating DOX had been stored in NPs. The loaded efficiency was estimated to be 30.5 mg DOX/100 mg NPs. The high loading capacity was attributed to strong electrostatic

interactions between positively charged DOX and negatively charged mTiO$_2$ of large surface area in neutral condition. The zeta
40 potential of blank NPs determined in water was - 44.5 mV, after adsorbing DTDC it was nearly stable at - 41.3 mV, whereas further loading DOX made it sharply increased to - 28.3 mV (**Fig. S5**). This indicated that during SERS generation process DTDC did not occupy the mesopores of mTiO$_2$, while DOX did in the
45 drug loading process.

The *in vitro* drug release behavior was studied in pH 7.4 and 5.0 PBS buffers to simulate neutral environment of blood circulation and acidic condition in cellular endosomes, respectively. As shown in **Fig. 3c**, DOX release was a little faster
50 at pH 5.0 than that at pH 7.4, which might be because the solubility of DOX decreased with the increase of pH in aqueous solution and the poor solubility lagged the drug release process.[37] Furthermore, we used a 785 nm laser (400 mW) to irradiate DOX-loaded NP solution (pH 5.0) for 6 min at the beginning of
55 every 1 h. As shown in **Fig. 3d**, the drug release became faster, which increased from 24.5% (without laser treatment) to 47.7% in 8 h, and illustrated apparent laser "switch-on" release phenomenon. AuNR encapsulated in NPs converted NIR light to local heating, which dissociated the strong interactions between
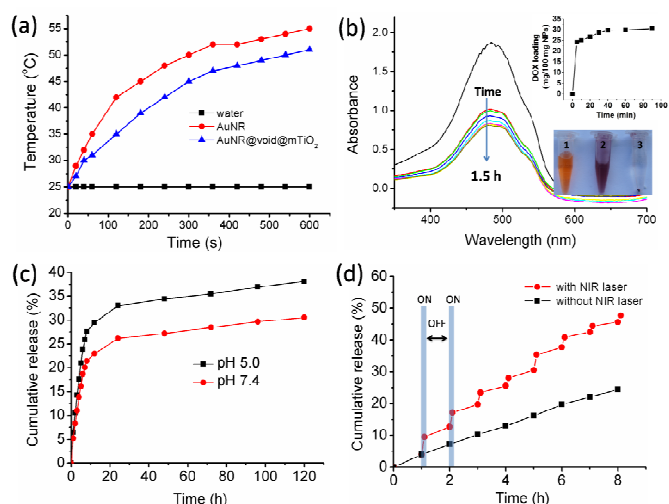60 DOX and mTiO$_2$ thus more DOX molecules were released.

Fig. 3. (a) Heating curves of water, AuNR and AuNR@void@mTiO$_2$ NP solutions with the same concentration of Au NR. The power of 785 nm laser
65 was 400 mW and the distance to Eppendorf tube filled with NP solution was 1 cm. (b) UV/Vis absorption spectra of DOX in separated supernatant solutions after various loading times with AuNR@void@mTiO$_2$ NPs. Inset: Loading profile of DOX with time and photographs of DOX solution (left), DOX-loaded NPs before (middle) and after (right) centrifugation. (c) DOX release
70 profiles from DOX-loaded NPs at different PBS solutions. (d) Comparison of DOX release profiles from DOX-loaded NPs with and without 785 nm NIR laser at PBS buffer (pH 5.0).

75 3.5. Structural Stability

Mesoporous NPs was good at drug loading due to the loose structure full of nanosized mesopores. Contradictory, such structure suffers from drawback of chemical and mechanical stabilities compared with the "solid" counterpart. It has been
80 reported that mSiO$_2$ can be severely degraded in a simulated physiological (pH 7.4 PBS buffer) condition,[38] which not only

influence it drug delivery capacity but also leave a potential risk for the biocompatibility. Lately researchers found that $mSiO_2$ NPs showed more apparent *in vivo* toxicity than solid SiO_2 NPs,[39] and degradation of $mSiO_2$ and the resultant products might be clues to explain this phenomenon. Considering the chemical inert feature of $mTiO_2$, we speculated that $mTiO_2$ had better stability in physiological condition. To prove this, our $AuNR@void@mTiO_2$ NPs were dispersed in pH 7.4 PBS buffer and gently stirred for 12 h at 37 °C. For comparison $AuNR@mSiO_2$ NPs were also subject to the same treatment. As expected, SEM images showed that $mSiO_2$ coating $AuNR@mSiO_2$ NPs dissolved to a large extent after the treatment , resulting in aggregated bare AuNR (**Fig. 4a,b**), condition was consistent with that of the reported work.[38] Whereas the structure of $AuNR@void@mTiO_2$ NP still kept compact (**Fig. 4c,d**). The difference was owing to Ti-OH was much stable than Si-OH in weak basic atmosphere. Take serial experimental results into account, it was essential for reexamination of the stability, biocompatibility, and the drug release mechanism of the $mSiO_2$ as a well-accept drug delivery material. In contrast, our $mTiO_2$ based nanomedicine held great advantage from the aspect of mechanical stability, which was first reported to the best of our knowledge.
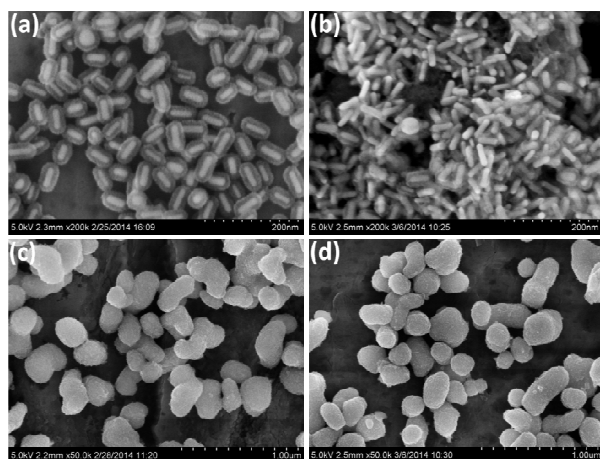

Fig. 4. (a) SEM images of $AuNR@mSiO_2$ NPs (a, b) and $AuNR@void@mTiO_2$ NPs (c, d) before (a, c) and after (b, d) stirring in pH 7.4 PBS buffer (0.01 M) at 37 °C for 12 h.

3.6. Optical Imaging

To verify the NPs' intracellular drug delivery ability, confocal laser scanning microscopy (CLSM) images of MCF-7 cells were taken after treatment with DOX-loaded NPs at different incubation time. As shown in **Fig. 5a**, very weak red fluorescence that resulted from DOX could be visualized in the cytoplasm after co-incubation for 1 h. When the incubation time was increased to 3 h, a much enhanced fluorescence was observed, indicating more NPs were taken up by tumor cell via endocytosis. Furthermore, we investigated the intracellular SERS performance of the drug-loaded NPs by a Raman microscopy equipped with a 632.8 nm laser. **Fig. 5b** showed the bright field images of the MCF-7 cells after NPs incubation. It was obvious that the NPs mainly distributed in cytoplasmic regions and almost no particles observed from nucleus, because the NPs were not small enough

to penetrate into nucleus. SERS spectra from different locations of one cell showed the strong signals appeared at cytoplasm while the signal at the nucleus was nearly undetected. Besides, the characteristic Raman signal of DTDC remained robust and no obvious interference Raman peaks were obtained due to the protection of $mTiO_2$ layer (**Fig. 5c**).

The *in vivo* SERS imaging performance of the NPs was evaluated in a mouse (**Fig. 5d**). A portion of 200 μL of the DOX-loaded NP solution was injected subcutaneously at the abdomen of an anaesthetized Kunming mouse. The subcutaneous SERS spectrum was detected using a 785 nm NIR laser excitation due to the satisfactory biological tissue penetration ability. As indicated in **Fig. 5e**, the spectral signatures of DTDC could be clearly distinguished at the injection location through the mouse skin, despite the intensity decreased to about half of that of pure NP solution. These results proved the high sensitivity of the SERS labeling holding great potential to be used for nanomedicine tracking studies in animal models.
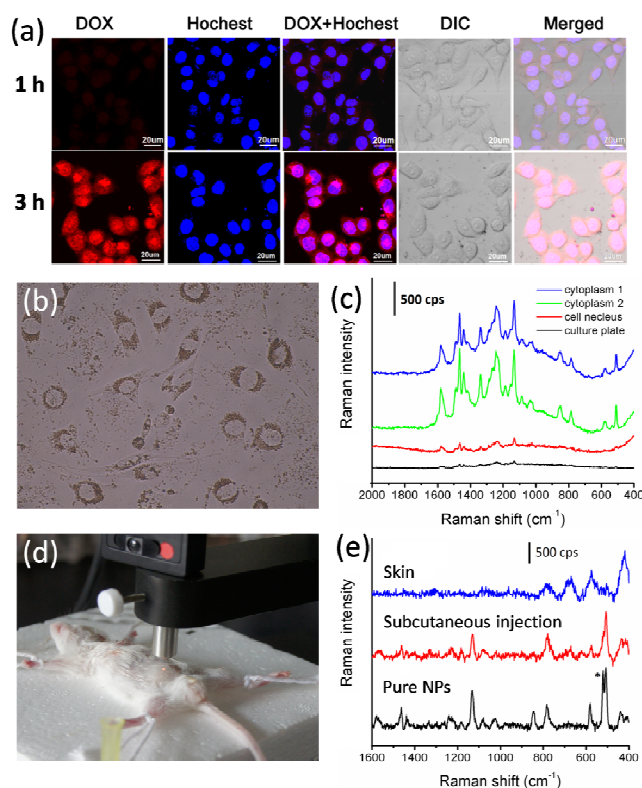

Fig. 5. (a) Confocal laser scanning microscopy images of MCF-7 cells taken after treatment with DOX-loaded NPs at different incubation time. Hoechst 33342 was used for cell nuclei staining (blue fluorescence). Red fluorescence in the MCF-7 cells was originated from DOX. (b) Bright field images of MCF-7 cells after incubating DOX-loaded $AuNR@void@mTiO_2$ NPs for 4 h and (c) corresponding Raman spectra at four different locations across one NP filled MCF-7 cell under 632.8 nm irradiation. (d) Photograph of a Kunming rat subcutaneously injected with 100 μL of DOX-loaded NP solution (0.2 mg mL^{-1}) under 785 nm excitation (200 mW). (e) SERS spectra from pure NP, the NP injected site and the blank skin. The peak at 520 cm^{-1} indicating with asterisk originated from the silicon wafer.

3.7. Therapeutic Property Studies

Next, we investigated the therapeutic properties of NPs and DOX-loaded NPs with and without laser irradiation via live/dead cell staining. As shown in **Fig. 6a**, both the cells after laser
5 exposure (6.25 W/cm^2) and incubation with blank NP (10 µg mL^{-1}) showed bright green fluorescence and no red fluorescence, indicated that the employed laser power density and blank NP did not cause any cell death. In contrast, laser irradiation of cells incubated with blank NPs or uptake of DOX-loaded NPs resulted
10 in decreased green fluorescence and sporadically distributed weak red fluorescence, indicating an unhealthy state of the cells. Laser irradiation of the cells with internalized DOX-loaded NPs resulted in severe cell death, as indicated by pale green and strong red fluorescence. These results preliminarily proved that cell
15 death was more effective when cells were incubated with drug-loaded NPs and irradiated with laser compared to all other cases.

To further evaluate the effectiveness of therapy using this multifunctional platform, MTT assay was employed to quantify the viability of MCF-7 cells treated with different conditions. It
20 was found that blank NPs exhibited little toxicity to cells even under high concentrations of 120 µg mL^{-1} after 24 hours of incubation (**Fig. 6b**). Considering the NP concentration dependent cytotoxicity and DOX loading content, a NP concentration of 10 µg mL^{-1} was fixed for the following
25 experiment. It could be seen that blank NPs incubation almost did not affect the cell viability (**Fig. 6c**). A suitable laser power density was also important, which should efficiently trigger the drug release and cell ablation functions at tumor site without damage normal cells. We applied a power density of 6.25 W/cm^2
30 to treat the blank MCF-7 cells (without NP) for 5 min and no obvious cytotoxicity was observed after 24 h incubation. Whereas the viability dramatically decreased to nearly 40.9% for NP filled cells upon NIR light irradiation, indicating as expected strong photothermal killing ability of NP. Furthermore, we compared the
35 cell killing efficacy free DOX and DOX-loaded NPs with and without NIR light irradiation. At the DOX concentration of 1 µM, free DOX and DOX-loaded NPs showed similar potency and about 50% of the cells were dead without light exposure. In comparison, DOX-loaded NPs under 5 min NIR irradiation killed
40 71.1% of the cells, illustrating an apparent chemo-photothermal synergistic effect.
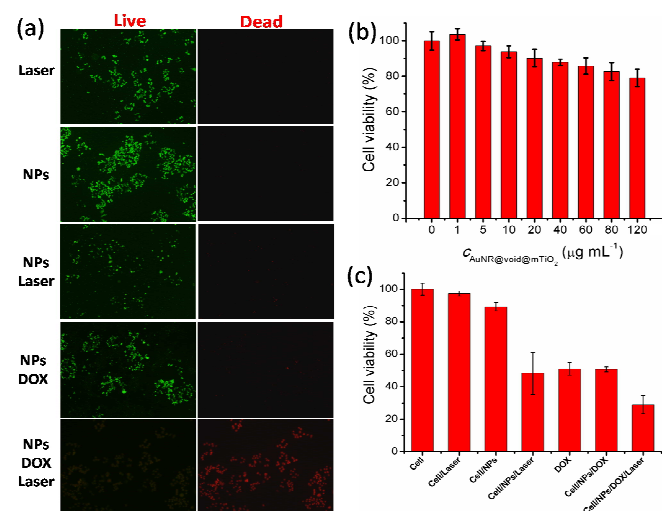

45 Fig. 6. (a) Live/dead cell monitoring of MCF-7 cells. All images collected after 60 min of incubation with 5-carboxyfluorescein diacetate/propidium iodide live/dead staining reagent. Cells showed a bright green fluorescence is an indication that the cells are alive. Cells exhibited neither red nor green fluorescence was an indication of an unhealthy state
50 of cells. (b) Cell viability of AuNR@void@mTiO$_2$ NPs against MCF-7 cells at different concentrations for 24 h. (c) Cell viabilities of MCF-7 cells in the presence of laser, blank NPs (10 µg mL^{-1}), NPs upon laser irradiation and those incubated with 1 µM DOX with and without irradiation. The power density of 785 nm laser as 6.25 W/cm^2 and the
55 exposure time was 5 min.

4. Conclusions

We have successfully prepared novel yolk-shell
60 AuNR@void@mTiO$_2$ NPs as theranostic tools for simultaneous SERS imaging and chemo-photothermal therapy. The interesting nanostructure, multifunction and terrific structural stability achieved taking advantage of multiple special features of AuNR, mSiO$_2$ and mTiO$_2$. Taking advantage of the novel and versatile "up to down" SERS labeling strategy, bright SERS signal was
65 obtained from NPs, which was successfully to be used for intracellular imaging and in vivo monitoring. Compared with chemotherapy or photothermal treatment, the combined treatment showed a synergistic effect, resulting in higher therapeutic efficacy. This proof-of-concept work aimed to provide a versatile
70 Raman reporter and drug co-loading strategy for developing SERS guided nanomedicine, and the NPs were directly used without surface functionalization before the cell culture and *in vivo* administration. Namely, the interaction with biological system was non-specific. We believed that if the
75 NPs were PEGylated and targeting moieties labeled, the long circulation in the body and tumor targeting properties would be achieved, making the nanoplatform applicable for *in vivo* tumor SERS imaging and cancer treatment.

Acknowledgements

100

† *School of Pharmacy, Yantai University, Yantai 264005, China*
§ *Key Laboratory of Coastal Environmental Processes and Ecological Remediation, Yantai Institute of Coastal Zone Research, Chinese Academy of Sciences, Yantai 264003, China. E-mail address:*
5 *yqwang@yic.ac.cn (Y.Q. Wang); lxchen@yic.ac.cn (L.X. Chen); Fax: +86 535 2109130; Tel: +86 535 2109130*

*Corresponding author.

Notes and references

10 1. D. E. Lee, H. Koo, I. C. Sun, J. H. Ryu, K. Kim and I. C. Kwon, *Chem. Soc. Rev.*, 2012, **41**, 2656–2672.
2. Y. Q. Wang and L. X. Chen, *Nanomedicine-NBM*, 2011, **7**, 385–402.
3. X. Yang, X. Liu, Z. Liu, F. Pu, J. Ren and X. Qu, *Adv. Mater.*, 2012, **24**, 2890–2895.
15 4. D. Lin, T. Qin, Y. Wang, X. Sun and L. Chen, *ACS Appl. Mater. Interfaces*, 2014, **6**, 1320–1329.
5. M. P. Melancon, M. Zhou and C. Li, *Acc. Chem. Res.*, 2011, **44**, 947–956.
6. W. Fang, Z. Wang, S. Zong, H. Chen, D. Zhu, Y. Zhong and Y. Cui,
20 *Biosens. Bioelectron.*, 2014, **57**, 10–15.
7. A. M. Fales, H. Yuan and T. Vo-Dinh, *Langmuir.*, 2011, **27**, 12186–12190.
8. K. V. Kong, Z. Lam, W. D. Goh, W. K. Leong and M. Olivo, *Angew. Chem. Int. Ed.*, 2012, **51**, 9796–9799.
25 9. Y. Zhang, J. Qian, D. Wang, Y. Wang and S. He, *Angew. Chem. Int. Ed.*, 2013, **52**, 1148–1151.
10. A. M. Fales, H. Yuan and T. Vo-Dinh, *Mol. Pharm.*, 2013, **10**, 2291–2298.
11. Y. Wang, B. Yan and L. Chen, *Chem. Rev.*, 2013, **113**, 1391–1428.
30 12. X. Niu, H. Chen, Y. Wang, W. Wang, X. Sun and L. Chen, *ACS Appl. Mater. Interfaces*, 2014, **6**, 5152–5160.
13. H. Abramczyk and B. Brozek-Pluska, *Chem. Rev.*, 2013, **113**, 5766–5781.
14. S. Schlucker, *Angew. Chem. Int. Ed.*, 2014, **53**, 4756–4795.
35 15. J. Song, L. Pu, J. Zhou, B. Duan and H. Duan, *ACS Nano*, 2013, **7**, 9947–9960.
16. G. von Maltzahn, A. Centrone, J. H. Park, R. Ramanathan, M. J. Sailor, T. A. Hatton and S. N. Bhatia, *Adv. Mater.*, 2009, **21**, 3175–3180.
40 17. L. Tian, N. Gandra and S. Singamaneni, *ACS Nano*, 2013, **7**, 4252–4260.
18. W. T. Lu, A. K. Singh, S. A. Khan, D. Senapati, H. T. Yu and P. C. Ray, *J. Am. Chem. Soc.*, 2010, **132**, 18103–18114.
19. Z. Zhang, L. Wang, J. Wang, X. Jiang, X. Li, Z. Hu, Y. Ji, X. Wu and
45 C. Chen, *Adv. Mater.*, 2012, **24**, 1418–1423.
20. S. Shen, H. Tang, X. Zhang, J. Ren, Z. Pang, D. Wang, H. Gao, Y. Qian, X. Jiang and W. Yang, *Biomaterials.*, 2013, **34**, 3150–3158.
21. J. Liu, S. Z. Qiao, J. S. Chen, X. W. Lou, X. R. Xing and G. Q. Lu, *Chem. Commun.*, 2011, **47**, 12578–12591.
50 22. K. C. Wu, Y. Yamauchi, C. Y. Hong, Y. H. Yang, Y. H. Liang, T. Funatsu and M. Tsunoda, *Chem. Commun.*, 2011, **47**, 5232–5234.
23. B. Nikoobakht and M. A. El-Sayed, *Chem. Mater.*, 2003, **15**, 1957–1962.
24. I. Gorelikov and N. Matsuura, *Nano Lett.*, 2008, **8**, 369–373.
55 25. A. F. Demirors, A. van Blaaderen and A. Imhof, *Langmuir.*, 2010, **26**, 9297–9303.
26. Y. Wang, L. Chen and P. Liu, *Chem. Eur. J.*, 2012, **18**, 5935–5943.
27. A. F. Demirors, A. van Blaaderen and A. Imhof, *Chem. Mater.*, 2009, **21**, 979–984.
60 28. I. Lee, J. B. Joo, Y. Yin and F. Zaera, *Angew. Chem. Int. Ed.*, 2011, **50**, 10208–10211.
29. S. Kim, Y. Jang, W. K. Oh, C. Kim and J. Jang, *Adv. Healthc. Mater.*, 2014, **3**, 1097–1106.
30. L. Zhang, T. Wang, L. Yang, C. Liu, C. Wang, H. Liu, Y. A. Wang
65 and Z. Su, *Chemistry - A European Journal*, 2012, **18**, 12512–12521.
31. L. M. Liz-Marzan, M. Giersig and P. Mulvaney, *Langmuir.*, 1996, **12**, 4329–4335.
32. G. B. Braun, S. J. Lee, T. Laurence, N. Fera, L. Fabris, G. C. Bazan, M. Moskovits and N. O. Reich, *J. Phys. Chem. C*, 2009, **113**, 13622–
70 13629.
33. M. Roca and A. J. Haes, *J. Am. Chem. Soc.*, 2008, **130**, 14273–14279.
34. J. Yang, D. Shen, L. Zhou, W. Li, J. Fan, A. M. El-Toni, W. X. Zhang, F. Zhang and D. Zhao, *Adv. Healthc. Mater.*, 2014, DOI: 10.1002/adhm.201400053
75 35. L.-L. Tay, P.-J. Huang, J. Tanha, S. Ryan, X. Wu, J. Hulse and L.-K. Chau, *Chem. Commun.*, 2012, **48**, 1024–1026.
36. C. Kim, S. Kim, W. K. Oh, M. Choi and J. Jang, *Chem. Eur. J.*, 2012, **18**, 4902–4908.
37. L. B. Chen, F. Zhang and C. C. Wang, *Small*, 2009, **5**, 621–628.
80 38. K. Chen, J. Zhang and H. Gu, *J. Mater. Chem.*, 2012, **22**, 22005–22012.
39. S. Lee, M. S. Kim, D. Lee, T. K. Kwon, D. Khang, H. S. Yun and S. H. Kim, *Int. J. Nanomedicine*, 2013, **8**, 147–158.

Nanoscale Accepted Manuscript